A HYBRID GYROKINETIC ION – FLUID ELECTRON MODEL FOR EDGE PLASMA SIMULATIONS

M. DORF, M. DORR, D. GHOSH, and M. UMANSKY
Lawrence Livermore National Laboratory
Livermore, California 94550, USA
Email: dorf1@llnl.gov

Abstract

The present work reports on the results of recent COGENT simulations performed with a hybrid gyrokinetic ion – fluid electron model in a diverter geometry. COGENT is a finite-volume code being developed for edge plasma modeling that employs a locally field-aligned coordinate system combined with a mapped multi-block grid technology to effectively handle strongly anisotropic turbulence in an X-point geometry. The simulation model solves the long-wavelength limit of a 5D full-F gyrokinetic equation for the ion species coupled to a 3D quasi-neutrality equation for the vorticity variable and an isothermal fluid electron response. The fluid part of the system contains fast electron-physics time scales and is therefore handled by making use of implicit time integration. The kinetic part of the system that involves ion transient and diamagnetic drift frequencies is typically treated explicitly with an implicit option for ion advection in case small-size cells are present in the computational mesh. The hybrid model includes ion scale ion temperature gradient (ITG) and resistive drift and ballooning modes as well as neoclassical ion physics and orbit loss effects. Preliminary results demonstrate formation of an Er-well and a modest density pedestal in the regime of suppressed turbulence for the case of a model single-null geometry and plasma parameters. In addition, first proof-of-principle simulations are performed for realistic parameters characteristic of the DIII-D experiment.

1. INTRODUCTION

The complexity of tokamak edge plasma dynamics, which involves multiple spatial and temporal scales, motivates the development of reduced modeling capabilities. In particular, gyrokinetic simulations of ion-scale, $k_\perp \rho_i \lesssim 1$, transport phenomena such as neoclassical transport or ion-scale (e.g., ITG, KBM) turbulence can greatly benefit from reduced electron models. Here, ρ_i is the ion gyro-radius and $k_\perp^{-1}$ represents the characteristic length-scale for variations in electromagnetic field perturbations. Indeed, including electron kinetic species into a simulation model introduces fast time scales, e.g., rapid parallel electron streaming, which are not coupled to the time scale of interest, e.g., drift frequency. As a result, one must either use an unnecessarily small time step for the stability of explicit time integration or develop a computationally expensive implicit time integration scheme.

To avoid numerical challenges related to kinetic electron effects, ion-scale gyrokinetic calculations of a tokamak core plasma have been successfully utilizing the reduced Boltzmann electron model, $n_e = \langle n_{i0} \rangle (1 + e\Phi/T_e - e\langle\Phi\rangle/T_e)$. Here, $\langle ... \rangle$ denotes the magnetic flux surface average, Φ is the electrostatic potential, n_{i0} is the initial ion density, and the electron temperature T_e is assumed to be a constant on the flux surfaces. This model, however, cannot be straightforwardly extended to the counterpart edge gyrokinetic simulations that span the magnetic separatrix. From the physical point of view, the Boltzmann model manifests a constant-in-time flux surface average of the electron density, $\partial\langle n_e \rangle/\partial t \equiv 0$, which, on closed flux surfaces, is equivalent to the zero-flux surface average of the electron radial particle flux. While the condition, $\partial\langle n_e \rangle/\partial t \equiv 0$, is approximately valid in a core region, such constraint is not applicable to the SOL plasmas due to the presence of large electron parallel losses to divertor plates. From the mathematical point of view, one can also notice that the flux surface average operator acting on the potential perturbations $\langle\Phi\rangle$ is discontinuous across the separatrix.

Although the Boltzmann electron model cannot be straightforwardly applied to gyrokinetic edge simulations, the next level in the hierarchy of increasingly detailed electron models – the drift-fluid model – can be used to improve the efficiency of ion-scale transport modeling in a tokamak edge [1-4]. Note that in the outer edge region the electrons are sufficiently cold such that their collision rate, ν_e, may be larger than their transit frequency, $\nu_e > V_{Te}/qR_0$, thereby justifying the electron fluid response. Here, q is the magnetic safety factor, R_0 is the tokamak major radius, and V_{Te} is the thermal velocity. A drift-fluid model includes the effects of finite plasma conductivity, allowing it to capture resistive drift modes. These modes are omitted in the collisionless Boltzmann model used for a hot, weakly-collisional core region. It is, however, important to note that the standard fluid treatment of the electrons does not incorporate trapped-electrons physics, which play a pronounced role in a less-collisional inner edge region. Consequently, these models omit the effects of trapped electron modes (TEM), which can be of

importance, for instance, in understanding L-mode turbulence and the L-H transition process. Another limitation of fluid models is their inability to account for parallel kinetic electron effects, which can be significant when estimating plasma heat fluxes on diverter plates.

It is instructive to note that drift fluid models employed for both electron and ion species have been routinely utilized in various mature 3D fluid codes for tokamak edge modeling [5-7]. However, these computational tools omit ion kinetic effects such as prompt orbit losses and neoclassical transport that can strongly influence the background radial electric field and intrinsic toroidal rotation – the effects that regulate edge plasma turbulence and transport. On the other hand, a hybrid model that includes gyrokinetic ion species and fluid electron species captures these important kinetic ion effects. Moreover, because fast electron time scales are contained within the 3D fluid/field part of the hybrid system, it is much less computationally expensive to perform implicit time integration for a low-dimensional fluid-electron system as compared to a high-dimensional kinetic-electron system. The 5D kinetic ion part of the hybrid model contains only the time scales of interest and is therefore treated explicitly. We note that in some cases, the computational intensity of performing an implicit time step for a 3D fluid/fields part of the hybrid system can be comparable to that of an explicit time step for a 5D ion kinetic part, thereby minimizing performance overhead for including ion kinetic effects.

A hybrid gyrokinetic ion – fluid electron approach for plasma edge simulations has been implemented in the finite-volume COGENT code [3-4]. COGENT is distinguished by its use of a locally field-aligned coordinate system combined with a mapped multi-block grid technology to effectively handle strongly anisotropic turbulence in an X-point geometry. The electrostatic hybrid model solves the long-wavelength limit of a full-F gyrokinetic equation for the ion species coupled to a quasi-neutrality equation for the vorticity variable and an isothermal fluid electron response. The implicit-explicit approach is applied to the numerical time integration, in which the fluid part of the problem, i.e., the vorticity equation, is treated implicitly and the gyrokinetic ion equation is advanced by making use of the standard explicit methods. The computational model was first applied to axisymmetric 4D/2D simulations of edge plasma transport [8], and then was extended to 5D/3D simulations of ion-scale turbulence [3-4]. The hybrid model includes ion scale ion temperature gradient (ITG) and resistive drift and ballooning modes as well as neoclassical ion physics and prompt orbit losses. The 5D/3D COGENT simulations performed for a model single-null geometry and plasma parameters in Ref. [4] explored the roles of a self-consistent background electric field and an X-point geometry by comparing cross-separatrix simulations with toroidal annulus counterpart simulations. In addition, the properties of neoclassical and turbulent transport were elucidated by comparing the results from the corresponding 5D/3D and 4D/2D COGENT simulations [4]. In the present work we report on the results of recent COGENT simulations exploring formation of an Er-well and density pedestal depending on the intensity of the resistive turbulence that is controlled by a prescribed conductivity parameter. The preliminary results obtained for a model geometry and plasma parameters demonstrate an increase of the Er-well and steepening of a density gradient in the case of weaker turbulence. In addition, proof-of-principle results for the realistic plasma parameters and magnetic geometry characteristic of the DIII-D experiment are reported. Finally, we present initial results from the development of an implicit numerical capability to handle the gyrokinetic advection operator. This implicit option can facilitate X-point simulations for the case where small-size cells are present in the computational mesh. It can also be useful for 4D/2D simulations, where a transport time-scale steady-state solution is of interest. The present paper is organized as follows: The numerical model is given in Sec. II, the simulation results are presented in Sec. III, and finally, the conclusions are summarized in Sec. IV.

2. NUMERICAL MODEL

The COGENT simulation model and numerical algorithms are described in detail in Ref. [3], and we only provide a brief summary here. The code solves a conservative form of a 5D full-F ion gyrokinetic equation in the long-wavelength limit:

$$\frac{\partial B_\parallel^* f_i}{\partial t} + \boldsymbol{\nabla}_{\mathbf{R}} \cdot \left(\dot{\boldsymbol{R}} B_\parallel^* f_i\right) + \frac{\partial}{\partial \mathrm{v}_\parallel}\left(\dot{\mathrm{v}}_\parallel B_\parallel^* f_i\right) = C_{ii}[B_\parallel^* f_i]. \tag{1}$$

Here, $f_i(\boldsymbol{R}, \mathrm{v}_\parallel, \mu)$ denotes the ion gyroaveraged distribution function, $\mathbf{R}$ is the gyrocenter coordinate, $\nabla_{\mathbf{R}}$ is the gradient with respect to $\mathbf{R}$, and the phase-space guiding-centre velocity is given by

$$\dot{\boldsymbol{R}} = \frac{1}{B_{\parallel}^{*}}\left[\mathrm{v}_{\parallel}\mathbf{B}^{*} + \frac{1}{Z_i e}\mathbf{b}\times(Z_i e\boldsymbol{\nabla}\Phi + \mu\boldsymbol{\nabla}B)\right], \tag{2}$$

$$\dot{\mathrm{v}}_{\parallel} = -\frac{1}{m_i B_{\parallel}^{*}}\mathbf{B}^{*}\cdot(Z_i e\boldsymbol{\nabla}\Phi + \mu\boldsymbol{\nabla}B), \tag{3}$$

where m_i and Z_i are the ion species mass and charge state, respectively, e is the electron charge, $\mathbf{B}(\mathbf{R}) = B\mathbf{b}$ is the magnetic field with $\mathbf{b}$ denoting the unit vector along the field, $\mathbf{B}^{*}(\mathbf{R},\mathrm{v}_{\parallel}) \equiv \mathbf{B} + (m_i c/Z_i e)\mathrm{v}_{\parallel}\boldsymbol{\nabla}\times\mathbf{b}$, $B_{\parallel}^{*}(\mathbf{R},\mathrm{v}_{\parallel}) \equiv \mathbf{B}^{*}\cdot\mathbf{b}$. The term on the right-hand-side (RHS) of Eq. (1) denotes the ion-ion collision operator. A range of increasingly detailed collision models including fully-nonlinear Fokker-Plank operator [9] are available in the code. For simplicity, in this work (in Sec. III. 1) we use a Lenard–Bernstein collision model [10]. Its numerical implementation in the COGENT code is described in Refs. [4,11].

Self-consistent variations of an electrostatic potential are described by making use of the quasi-neutrality equation ($\nabla\cdot\boldsymbol{j} = 0$) for the vorticity variable

$$\varpi = \boldsymbol{\nabla}_{\perp}\cdot\left(\frac{c^2 n_i m_i}{B^2}\boldsymbol{\nabla}_{\perp}\Phi\right), \tag{4}$$

$$\frac{\partial\varpi}{\partial t} + \boldsymbol{\nabla}\cdot\left(c\frac{-\boldsymbol{\nabla}\Phi\times\mathbf{B}}{B}\varpi\right) = \boldsymbol{\nabla}\cdot\left(\frac{2\pi Z_i e}{m_i}\int \mathbf{v}_{\perp}^{m} f_i B_{\parallel}^{*} d\mathrm{v}_{\parallel} d\mu\right) + \boldsymbol{\nabla}\cdot\left[\frac{cZ_i n_i T_e}{B}\left(\boldsymbol{\nabla}\times\mathbf{b} + \frac{\boldsymbol{b}\times\boldsymbol{\nabla}B}{B}\right)\right] + \boldsymbol{\nabla}\cdot\left[\mathbf{b}\sigma_{\parallel}\left(\frac{1}{eZ_i n_i}\nabla_{\parallel}(n_e T_e) - \nabla_{\parallel}\Phi + \frac{0.71}{e}\nabla_{\parallel}T_e\right)\right]. \tag{5}$$

Here, $\mathbf{v}_{\perp}^{m} \equiv \dot{\boldsymbol{R}}_{\perp}(\Phi = 0)$ is the magnetic drift velocity corresponding to the perpendicular component of the guiding centre velocity in Eq. (2) for the case of a zero potential, $\sigma_{\parallel} = 1.96 n_e e^2\tau_e/m_e$ is the parallel electron conductivity, with τ_e denoting the basic electron collisional term given by Braginskii. The vorticity equation [Eq. (5)] assumes the long-wavelength approximation, $k_{\perp}\rho_i \ll 1$, which is roughly consistent with the longer-wavelength nature of edge turbulence, $10^{-2} \ll k_{\perp}\rho_s < 1$ [12]. Here, $\rho_s = \omega_{ci}^{-1}V_s = \omega_{ci}^{-1}\sqrt{T_e/m_i}$ is the ion sound gyroradius. For numerical stability purposes it was, however, found important to retain $k_{\perp}^2\rho_s^2$ polarization density correction, i.e.,

$$n_e = \boldsymbol{\nabla}_{\perp}\cdot\left(\frac{c^2 n_i m_i}{eB^2}\boldsymbol{\nabla}_{\perp}\Phi\right) + Z_i n_i, \tag{6}$$

in the divergence of the parallel current term [the last term on the RHS of Eq. (5)]. That correction provides stabilization of high-$k_{\perp}\rho_s$ perturbations, which are not resolved by the grid and can otherwise destabilize simulations. Note that the polarization correction is neglected in the divergence of the perpendicular diamagnetic electron current [the second term on the RHS of Eq. (5)] and in the denominator of the parallel pressure gradient term, $\nabla_{\parallel}(n_e T_e)/eZ_i n_i$. The vorticity equation [Eq. (5)] explicitly includes the Reynolds stress term, which can therefore be turned on or off in order to assess its influence on critical processes in edge plasmas, e.g., the L-H transition process. This is in contrast to standard gyrokinetic models that incorporate both kinetic ion and electron responses [13-14], where the effect of Reynolds stress forces is implicit – manifesting itself through the evolution of plasma species density. The parallel advection of the vorticity variable is omitted in Eq. (5) for simplicity. The vorticity equation needs to be coupled to a model for the electron temperature. In the present work, a prescribed electron temperature profile, $T_e(\mathbf{R},t) = T_e(\psi)$ is used, where ψ is the magnetic flux function. Finally, we note that Eq. (6) contains a fast time scale associated with high values of electron conductivity, $\tau_{cond}\sim(k_{\perp}^2\rho_s^2)\tau_e(k_{\parallel}V_{Te}\tau_e)^{-2}$, and an implicit time integration approach is used in COGENT to "step over" this time scale [3].

The quasi-neutrality model in Eqs. (4)-(6) appears similar to vorticity models adopted in drift-reduced fluid simulations (see, for instance, Ref. [5]). However, here it employs the ion gyrokinetic equation to evaluate the perpendicular ion current, thereby retaining important kinetic ion effects such as prompt X-point losses. It is instructive to note that the standard drift-fluid formulations are written in terms of the electron density, n_e, and not the ion gyrocenter density, n_i [see Eq. (6)]. Therefore, the polarization correction term does not appear in the equation for the parallel current density (see Eq. (5) in Ref. [5]). On the other hand, the divergence of the parallel current, which provides high-$k_{\perp}\rho_s$ stabilization, is included in the continuity equation for the plasma, i.e., electron, density (see Eq. (2) in Ref. [5]).

A hybrid gyrokinetic ion – drift fluid electron approach was previously used in simulations of a tokamak core plasma performed with the GEM [1] and XGC [2] gyrokinetic codes. However, the gyro-Poisson model [see Eq. (6)] was employed instead of the vorticity (quasi-neutrality) formulation [see Eq. (5)]. We believe that the vorticity formulation, can be beneficial for numerical simulations. Specifically, it directly incorporates the $\boldsymbol{\nabla} \cdot (\boldsymbol{b} \cdot j_{\|})$ term, allowing for discretization methods that can minimize numerical pollution associated with the possible non-zero discrete nature of $\langle \boldsymbol{\nabla} \cdot (\boldsymbol{b} \cdot j_{\|}) \rangle$ [3]. Moreover, it facilitates the straightforward implementation of a preconditioner to enhance the efficiency of implicit time integration [3-4].

The ion gyrokinetic equation [Eq. (1)] is to be solved subject to an inflow-flux boundary condition. In the present work, inflow fluxes are generated by a Maxwellian "bath" located at a domain boundary and characterized by specified values for density, temperature, and parallel momentum. Those values are typically chosen to be consistent with the initial plasma profiles. Boundary conditions for the electrostatic potential include a zero Dirichlet boundary condition on all domain boundaries except for the inner radial (core) boundary, where the following boundary condition is applied [3]

$$\langle \frac{c^2 n_i m_i}{B^2} |\boldsymbol{\nabla}\psi|^2 \rangle \frac{\partial \Phi}{\partial \psi} = \int_0^t dt \langle \boldsymbol{\nabla}\psi \cdot \boldsymbol{j}_i \rangle . \quad (7)$$

Here, $j_i = (2\pi Z_i e/m_i) \int \dot{\boldsymbol{R}} f_i B_{\|}^* d\mathrm{v}_{\|} d\mu$ is the ion gyrocenter current density and $\langle \ldots \rangle$ denotes the flux surface average operator. The boundary condition in Eq. (7) allows for consistent development of the long-wavelength background radial electric field at the radial boundaries, while plausibly mitigating near-boundary turbulence by suppressing short-wavelength poloidal variations in Φ. To further stabilize near-boundary behavior in the simulations discussed in Sections 3.1 and 3.2, an ad-hoc poloidal dissipation term is applied to the vorticity variable within a narrow radial layer at the radial boundaries.

3. SIMULATION RESULTS

In this section we present the results of gyrokinetic ion – drift fluid electron COGENT simulations performed for the model (Sec. 3.1) and DIII-D (Sec. 3.2) plasma parameters. Then, in Sec. 3.3 we report on the development of an implicit numerical capability for handling the gyrokinetic advection operator, which can be used to improve the performance of hybrid-model simulations.

3.1. Simulations with model geometry and plasma parameters

A model X-point magnetic geometry shown in Fig. 1 (see, Ref. [4] for a detailed description) closely matches a concentric toroidal annulus geometry inside the separatrix. This geometry is employed in COGENT simulations to assess the role of the X-point by comparing cross-separatrix simulations with toroidal annulus counterpart simulations. To reduce the computational intensity of 5D simulations, increased values of ion, T_i, and electron, T_e, temperatures can be considered. Numerical simulations that assumed, $T_i \sim T_e \sim 4$ keV were performed in Ref. [4] for the model plasma geometry to assess the role of X-point geometry, background E_r and plasma resistivity on edge turbulence properties. Those simulations, however, considered the case of a shallow plasma density gradient. Also, a rather large density value was used for a Maxwellian bath boundary condition at the divertor plates and outer radial boundary. As a result, a large ion inflow from the divertor plates and outer SOL boundary could provide pronounced compensation for the orbit loss effect. Nevertheless, development of a mild E_r-well near the last closed flux surface (LCFS) was observed [4].

Here, we extend the analysis in Ref. [4] by considering a steeper density gradient [Fig. 2(a)], lower Maxwellian bath density value for the ion inflow boundary flux, and a reduced value of an electron temperature, $T_e = 400$ eV. We perform simulations for two different values of a prescribed uniform parallel conductivity, $\sigma_{\|} = 1.96 N_0 e^2 \bar{\tau}_e / m_e$, corresponding to $\bar{\tau}_e V_{T_e}/(\bar{q} R_0) = 0.14$ (high conductivity) and $\bar{\tau}_e V_{T_e}/(\bar{q} R_0) = 0.094$ (low conductivity) to assess the influence of the resistive turbulence on the formation of a density pedestal and E_r-well. Here, $\bar{q} = 2.5$ is the characteristic value of the magnetic safety factor and $R_0 = 1.6$ m is a major radius. Details about the computational domain, grid resolution, ion-ion collisions and the functional form for initial profiles can be found in Ref. [4] and are also mentioned in the caption to Fig. 1.

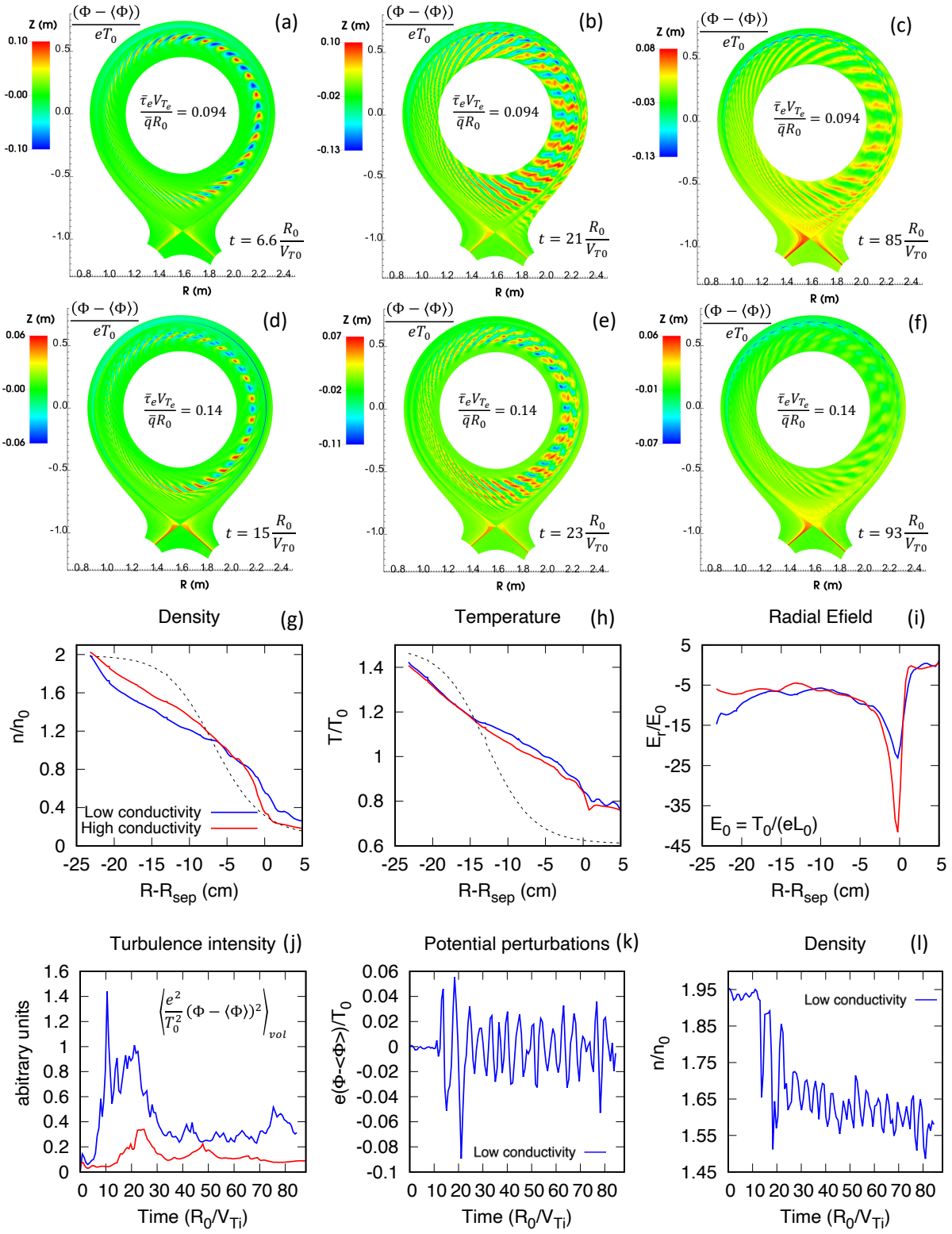

FIG. 1. Results of the COGENT simulations in a model geometry for a single-charge deuterium plasma with an increased ion temperature, T_0=4 keV. Frames (a)-(c) and (d)-(f) illustrate electrostatic potential perturbations for the low-conductivity and high-conductivity cases, respectively. Outboard midplane lineouts and time history measured on the outboard midplane at 19 cm inside the separatrix are plotted in Frames (g)-(i) and (k)-(l), respectively. The dashed curves in Frames (g) and (h) show the initial plasma density and temperature profiles. The ion-ion collision frequency is taken uniform with $\nu_{ii} = 0.01V_{T0}/(\bar{q}R_0)$. *The computational-space volume average* $\langle\rangle_{vol}$ *in Frame (j) is defined as a sum over all spatial cells divided by the number of cells. A periodic toroidal wedge with the size* $2\pi/8$ *is simulated, the spatial grid resolution in core region corresponds to* $N_\psi = 76, N_\phi = 4, N_\theta = 512$, *and the velocity grid resolution is given by* $N_{v_\parallel} = 32, N_\mu = 24$. *A time step is limited by the explicit ion phase-space advection and is given by* $dt \sim 0.013R_0/V_{T0}$. *The toroidal magnetic field is specified by* $B_\phi R = 3.5\ T \cdot m$, *the major radius is* R_0=1.6 *m, and the normalization length parameter is* L_0=1 *m.*

Simulations in Fig. 1 illustrate that weaker turbulence corresponding to the low-conductivity case [Fig. 1(j)] correlates with a deeper E_r-well [Fig. 1(i)] and a stepper density gradient [Fig. 1(g)] in the edge region. Although the model plasma parameters and magnetic geometry are used, we emphasize that the simulations include the effects of neoclassical physics, prompt orbit losses, and ITG and resistive turbulence. This simulation set-up can therefore be used to develop an improved theoretical understanding of critical processes in a tokamak edge, such as the L-mode turbulence and L-H transition. For the latter analysis, it is important to improve the simulation model by adding an energy equation for the electron fluid temperature, which in turn should be used for the self-consistent calculation of plasma conductivity. These developments will be the subject of our future work.

3.2. Proof-of-principle simulations for realistic DIII-D parameters

Here, we demonstrate the results of proof-of-principle COGENT simulations [see Fig. 2] performed for the parameters characteristic of the DIII-D tokamak. The magnetic geometry and the initial profiles for the ion and electron temperature (the latter is maintained fixed) correspond to the parameters of the L-mode discharge #150142 reported in Ref. [15]. We note that the plasma profiles in Ref. [15] are only reported on closed field lines and an ad-hoc extrapolation is utilized here to initialize plasma profiles on open field lines. An increased initial ion density gradient (as compared to that reported in Ref. [15]) is adopted to enhance the intensity of the pressure-driven resistive turbulence. In contrast to the simulations described in the previous section (Sec. 3.1), here the parallel plasma conductivity is not uniform and is computed consistent with the prescribed electron temperature profile. We, however, impose an arbitrary limitation on the value of the electron collisional time, τ_e, in the expression for the Braginskii's conductivity by replacing it with the electron transit period, $\tau_e \to qR_0/V_{Te}$, in the hotter core region where $\tau_e > qR_0/V_{Te}$ and where Braginskii's collisional theory is of limited validity. Finally, for simplicity purposes and to further enhance the microturbulence, the Reynolds-stress term and ion-ion collisions are not included in the simulations.

The results of COGENT simulations are shown in Fig. 2. The simulation domain in the toroidal direction corresponds to a periodic wedge of $\Delta\phi_{wedge} = 2\pi/8$, and the grid resolution is given by $N_\psi = 80, N_\phi = 4, N_\theta = 2144, N_{v\parallel} = 32, N_\mu = 12$. The time step, dt~0.14 μs, is set by the Courant constraint for the ion advection operator and requires nine seconds of wall-time when executed on 1728 cores of the Cori NERSC cluster. It is interesting to note that for the considered parameters, strong turbulence cut-off at the magnetic separatrix is observed. Recall, that the present simulation model omits trapped electron modes and electromagnetic effects. The latter can be particularly important in a tokamak edge (including the present studies), where the Alfven transit frequency, V_A/qR_0, is comparable to the maximum drift frequency, $V_s/L_\perp$ [12]. Here, V_A and V_s are the Alfven and ion sound velocities, respectively, and $L_\perp$ is the length-scale of background plasma profiles.

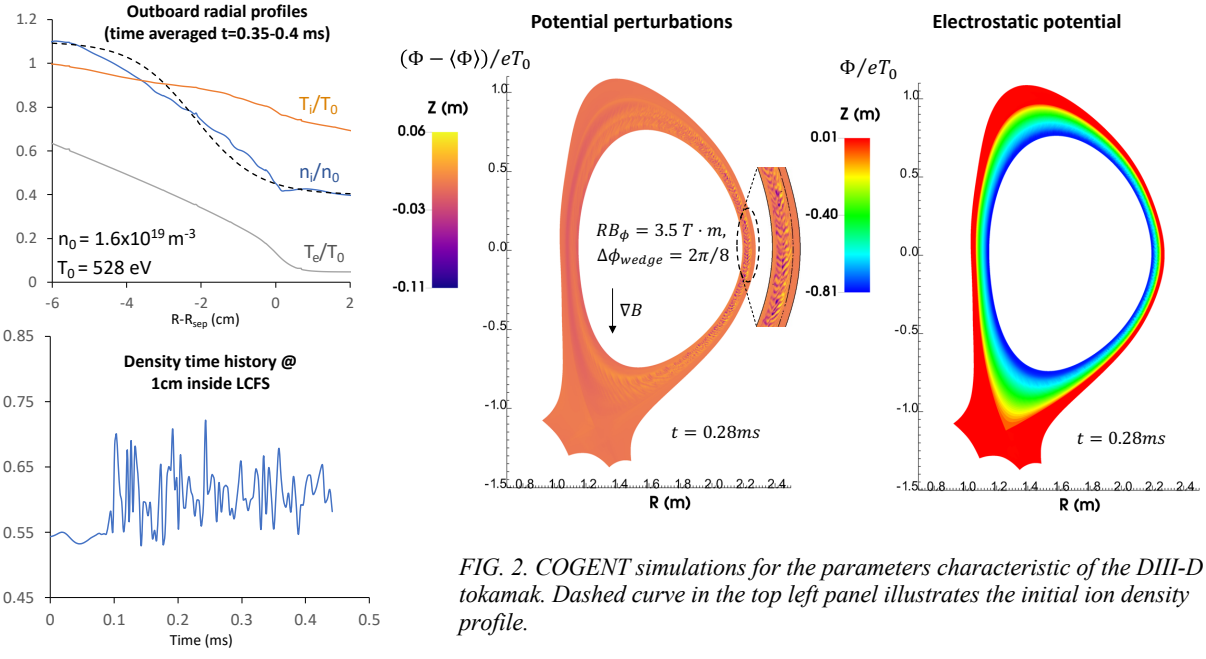

FIG. 2. COGENT simulations for the parameters characteristic of the DIII-D tokamak. Dashed curve in the top left panel illustrates the initial ion density profile.

3.3. Implicit capability for the gyrokinetic advection operator

The ion scale turbulence in a tokamak edge is characterized by the drift time scale $\tau_{dr} \sim L_\perp/[(k_\perp \rho_s)V_s]$ and wavelength spatial structures with $10^{-2} \ll k_\perp \rho_s < 1$ [12]. At the same time, the $E \times B$ drift velocity corresponding to the background radial electric field that balances the radial ion pressure gradient is given by $V_{E\times B} \sim \rho_i V_{Ti}/L_\perp$ on closed field lines. Typical edge-turbulence simulations adopt the perpendicular grid size of $\Delta x_\perp \sim \rho_i$, and therefore the CFL-limited time step $dt \sim L_\perp/V_{Ti}$ can be somewhat smaller than the characteristic time scale of interest, τ_{dr}. Moreover, the presence of an X-point can lead to small-size cells in a computational mesh. For instance, small poloidal-size cells near a gridline connecting O and X points occur for locally-orthogonal grids in the poloidal plane. Although poloidal grid orthogonality is abandoned in COGENT near the X-point, unnecessarily small cells can still appear due to geometrical complexities. This in turn leads to a tighter CFL constraint and non-optimal time integration properties. Other important applications, where an advection CFL-limited time step is much smaller than a time scale of interest include (a) 5D turbulence simulations with the non-field-aligned, toroidal (ψ, θ, ϕ) grid, which can be employed for verification purposes [16], and (b) 4D axisymmetric transport time scale simulations, where a transport steady-state is of interest [8].

The CFL limit for the advection operator has been traditionally circumvented in gyrokinetic codes by making use of the semi-Lagrange approach [17-18]. In the context of COGENT's implicit-explicit (ImEx) time integration framework, declaring the gyrokinetic Vlasov term as implicit results in the need to solve a 4D or 5D linear system to precondition the solution of the Jacobian system in the Newton-Krylov solves performed in each implicit stage. In addition to having the full phase space dimension, the coefficient matrix of this linear system is non-symmetric and indefinite. COGENT solves this linear system using the Approximate Ideal Restriction (AIR) option in the BoomerAMG algebraic multigrid solver contained in the Hypre linear solver library [19]. The use of multigrid methods to solve nonsymmetric indefinite systems has historically been highly problematic, but the recent development of the AIR approach, including several variants, provides a way to potentially extended the benefits of multigrid algorithms beyond the symmetric, positive-definite systems for which they are more commonly used.

To further enhance the efficiency of the implicit Vlasov solves, COGENT allows the preconditioner to be defined using a lower-order discretization than that used for the Vlasov operator itself. To achieve high-order temporal accuracy, third-order upwind (UW3), fifth-order upwind (UW5) and fourth-order BWENO options are routinely employed to discretize the Vlasov operator. For the UW3 and UW5 options, we observe that constructing the preconditioner using a first-order upwind scheme (UW1) provides a robust preconditioner even for relatively large time steps, while also yielding a sparser matrix. Because the BWENO option makes adaptive upwinding choices that cannot be easily reproduced in a lower-order preconditioner, this approach cannot be used for that case, however.

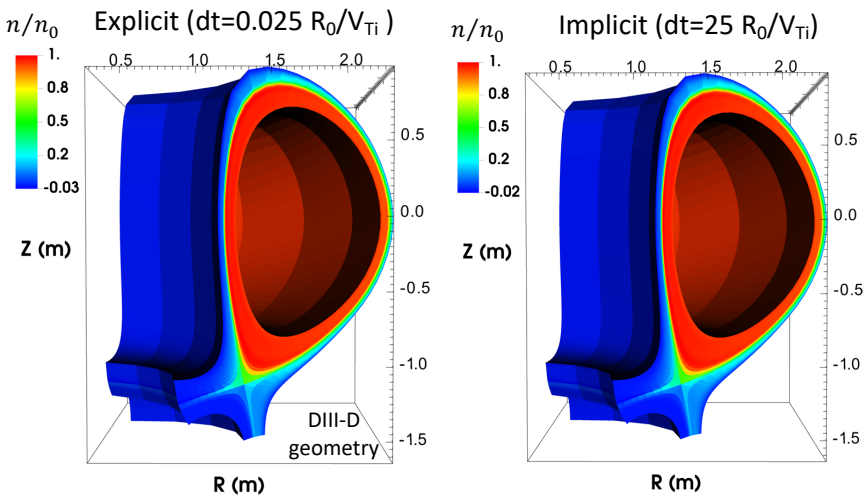

FIG. 3. Implicit (right) vs explicit (left) COGENT simulations for a passive gyrokinetic advection test case. Relaxation of an ion distribution function in the absence of electric fields and collisions is considered. Ion distribution with initially uniform density and temperature is being absorbed by the diverter plates and the outer radial boundary. Final steady-state is shown. Note the presence of a residual plasma density on open field lines due to the magnetic bottle effect. The factor of 20 in wall-clock runtime speed-up is observed.

4. CONCLUSIONS

This work presents the results of recent COGENT simulations performed using the electrostatic hybrid gyrokinetic ion – fluid electron model. The hybrid model is applied to study the properties of plasma transport in a single-null geometry. COGENT simulations performed for the model plasma parameters (with an increased ion temperature) and magnetic geometry demonstrate formation of a deeper Er-well and steeper edge density gradients consistent with a decrease in the intensity of the resistive turbulence. The latter is controlled in the present work by a prescribed value of the plasma conductivity. Additionally, proof-of-principle simulations for the realistic DIII-D parameters including consistent calculation of the plasma conductivity profile are presented. Finally, development of an implicit capability for the time integration of the gyrokinetic advection problem is reported.

ACKNOWLEDGEMENTS

This research was supported by the U.S. Department of Energy under contract DE-AC52-07NA27344.

REFERENCES

[1] PARKER, S., et al., Electromagnetic gyrokinetic-ion drift-fluid-electron hybrid simulation, Comput. Phys. Commun. **127** (2000) 59-70.
[2] HAGER, R., et al., Verification of long wavelength electromagnetic modes with a gyrokinetic-fluid hybrid model in the XGC code, Phys. Plasmas **24**, (2017) 054508.
[3] DORF, M., DORR, M., Continuum Gyrokinetic Simulations of Edge Plasmas in Single-Null Geometries, Phys. Plasmas, **28**, (2021) 032508.
[4] DORF, M., DORR, M., Modelling of electrostatic ion-scale turbulence in divertor tokamaks with the gyrokinetic code COGENT, Contrib. Plasma Phys. (2022); e202100162. https://doi.org/10.1002/ctpp.202100162.
[5] GALASSI, D., et al., Tokamak Edge Plasma Turbulence Interaction with Magnetic X-Point in 3D Global Simulations, Fluids **4**, (2019) 50.
[6] ZHOLOBENKO, W., et al., Electric field and turbulence in global Braginskii simulations across the ASDEX Upgrade edge and scrape-off layer, Plasma Phys. Control. Fusion **63** (2021) 034001.
[7] DUDSON, B., LEDDY, J., Hermes: global plasma edge fluid turbulence simulations, Plasma Phys. Control. Fusion **59** (2017) 054010.
[8] DORF, M., DORR, M., Continuum kinetic modelling of cross-separatrix plasma transport in a tokamak edge including self-consistent electric fields, Contrib. Plasma Phys. **58** (2018) 434-444.
[9] DORF, M., et al., Progress with the COGENT Edge Kinetic Code: Implementing the Fokker-Planck Collision Operator, Contrib. Plasma Phys. **54** (2014) 517-523.
[10] BERNSTEIN, I., LENARD, A., Plasma Oscillations with Diffusion in Velocity Space, Phys. Rev. **112** (1958) 1456.
[11] ANGUS, J., On Anomalous Plasma Transport in The Edge of Magnetic Confinement Devices, Ph.D. Thesis, University of California, San Diego, 2012.
[12] SCOTT, B., Three-dimensional computation of drift Alfven turbulence, Plasma Phys. Control. Fusion **39** (1997) 1635.
[13] CHANG, C.S., Fast Low-to-High Confinement Mode Bifurcation Dynamics in a Tokamak Edge Plasma Gyrokinetic Simulation, Phys. Rev. Lett. **118** (2017) 175001.
[14] MICHELS, D., Full-f electromagnetic gyrokinetic turbulence simulations of the edge and scrape-off layer of ASDEX Upgrade with GENE-X, Phys. Plasmas, **29** (2022) 032307.
[15] Data taken from the ATOM SciDAC use case DIII-D 150142, https://atom.scidac.io/usecase.html.
[16] DORF, M., DORR, Progress with the 5D full-F continuum gyrokinetic code COGENT, Contrib. Plasma Phys. (2020); e201900113. https://doi.org/10.1002/ctpp.201900113.
[17] GRANDGIRARD, V., et at., A 5D gyrokinetic full-f global semi-Lagrangian code for flux-driven ion turbulence simulations, Comput. Phys. Commun. **207** (2016) 35–68.
[18] BARNES, M., Stella: An operator-split, implicit–explicit δf-gyrokinetic code for general magnetic field configurations, J. Comput. Phys. **391** (2019) 365-380.
[19] HYPRE: Scalable Linear Solvers and Multigrid Methods. https://www.llnl.gov/casc/hypre/